Published in final edited form as:
Mol Cancer Ther. 2014 August ; 13(8): 2018–2029. doi:10.1158/1535-7163.MCT-14-0166.

Mechanism and efficacy of sub-50 nm tenfibgen nanocapsules for cancer cell-directed delivery of anti-CK2 RNAi to primary and metastatic squamous cell carcinoma

Gretchen M. Unger[1], **Betsy T. Kren**[2,3], **Vicci L. Korman**[1], **Tyler G. Kimbrough**[4], **Rachel I. Vogel**[3], **Frank G. Ondrey**[4], **Janeen H. Trembley**[3,5,6], and **Khalil Ahmed**[3,4,5,6,*]

[1]GeneSegues, Chaska, MN 55318

[2]Department of Medicine, University of Minnesota, Minneapolis, MN 55417

[3]Masonic Cancer Center, University of Minnesota, Minneapolis, MN 55417

[4]Department of Otolaryngology, University of Minnesota, Minneapolis, MN 55417

[5]Department of Laboratory Medicine and Pathology, University of Minnesota, Minneapolis, MN 55417

[6]Cellular and Molecular Biochemistry Research Laboratory (151), Minneapolis VA Health Care System, Minneapolis, MN 55417

Abstract

Improved survival for HNC patients with recurrent and metastatic disease warrants that cancer therapy is specific with protected delivery of the therapeutic agent to primary and metastatic cancer cells. A further objective should be that downregulation of the intracellular therapy target leads to cell death without compensation by an alternate pathway. To address these goals, we report the utilization of a sub-50 nm tenfibgen (s50-TBG) nanocapsule that delivers RNAi oligonucleotides directed against the essential survival signal protein kinase CK2 (RNAi-CK2) in a cancer cell-specific manner. We have evaluated mechanism and efficacy of using s50-TBG-RNAi-CK2 nanocapsules for therapy of primary and metastatic head and neck squamous cell carcinoma (HNSCC). s50-TBG nanocapsules enter cancer cells via the lipid raft/caveolar pathway and deliver their cargo (RNAi-CK2) preferentially to malignant but not normal tissues in mice. Our data suggest that RNAi-CK2, a unique single-stranded oligonucleotide, co-opts the argonaute 2/RNA induced silencing complex (Ago2/RISC) pathway to target the CK2αα' mRNAs. s50-TBG-RNAi-CK2 inhibited cell growth corresponding with reduced CK2 expression in targeted tumor cells. Treatment of three xenograft head and neck squamous cell carcinoma (HNSCC) models showed that primary tumors and metastases responded to s50-TBG-RNAi-CK2 therapy, with tumor shrinkage and 6-month host survival that was achieved at relatively low doses of the therapeutic agent without any adverse toxic effect in normal tissues in the mice. We suggest that

*Corresponding author: K. Ahmed, Cellular and Molecular Biochemistry Research Laboratory (151), Minneapolis VA Health Care System, One Veterans Drive, Minneapolis, MN 55417, USA. Telephone: (612)-467-2594. Fax: (612)-725-2093. ahmedk@umn.edu.

Disclosure of Potential Conflict of Interest: No conflicts to disclose.

our nanocapsule technology and anti-CK2 targeting combine into a therapeutic modality with a potential of significant translational promise.

Keywords

nanocapsule; nanoparticle; CK2; metastasis; survival

Introduction

Head and neck cancers (HNCs) represent approximately 3% of all cancers in the United States and 42,440 diagnoses of oral cavity and pharynx HNCs are expected for the year 2014 (1). In general, survival for HNC patients has not improved significantly over the last several decades because of the difficulties in treating recurrent and metastatic disease (2, 3). The use of Cetuximab, an epidermal growth factor receptor (EGFR)-specific antibody, in combination with chemotherapy extends median overall survival from 7.4 to 10.1 months in patients with recurrent or metastatic HNSCC (4) warranting more effective treatment approaches to address recurrent and disseminated disease.

Much recent work has pointed to the strong potential of targeting protein kinase CK2 for cancer therapy. CK2 (acronym for previous name casein kinase 2 or II) is a ubiquitous and highly conserved protein Ser/Thr kinase impacting a broad range of cellular activities that has led to the notion that it is a “master regulator” of cell function (5–7). The CK2 tetrameric complex consists of two catalytic α and/or α' subunits, encoded by separate genes, and two regulatory β subunits. This kinase is constitutively active and is localized both to the nuclear and cytoplasmic compartments of cells. The potential involvement of CK2 in cancer cell biology has long been recognized because of its role in cell proliferation and the observations that CK2 is elevated, predominantly at the protein or enzymic activity level relative to normal tissue, in all cancers that have been examined (6, 8–10). The role of CK2 in the cancer cell phenotype was firmly established when it was found that CK2 both stimulates cell growth and potently inhibits apoptosis —thus providing dual effects of promoting proliferation while inhibiting cell death (11, 12). The potential of CK2 as a therapeutic target was suggested by original studies that demonstrated that downregulation of CK2 by various molecular strategies resulted in death of cancer cells in vitro and in vivo (13–18); subsequently, the druggability of CK2 was also documented with the development of chemical inhibitors (19–21).

Increased CK2 expression in HNSCC is correlated with disease status and prognosis (8, 22, 23). Using immunohistochemical analysis of patient samples, elevated CK2 levels were strongly detected at the proliferating edge as well as throughout the tumor sections; in comparison, Ki-67 staining was detected only at the proliferating edge (22, 23). Together, mounting evidence on increased CK2 abundance and its shift toward nuclear accumulation throughout tumor sections suggests that CK2 dysregulation underpins the malignant processes of tumor growth and maintenance. In a previous report, we documented the role of CK2 in various HNSCC signaling pathways and showed that CK2 knockdown has a potent effect on several of these pathways (23).

For most molecular targets, a particularly important consideration for delivery of any cancer therapy agent remains the need for specific delivery to malignant cells. To that end, a large number of nanoparticle based delivery approaches have been devised (see e.g., (24)). These approaches have achieved varying degrees of success in precise targeting to cancer cells. Because CK2 is a ubiquitous and essential survival signal in normal as well as cancer cells, it is important to target it specifically in cancer cells to achieve a satisfactory response. Along these lines, we have utilized a novel nanocapsule that has the characteristics of directed targeting to cancer cells while avoiding the normal cells. The nanocapsule shell is comprised of tenfibgen, the carboxy-terminal fibrinogen globe domain of tenascin-C, surrounding therapeutic agents such as CK2 antisense or siRNA (10, 23–25). Important features of the nanocapsule are: a) the TBG ligand shell that allows receptor-mediated targeting to cancer cells via tenascin receptors which are elevated in these cells (26–31); b) avoidance of reticuloendothelial system (RES) accumulation; c) avoidance of endosomal/lysosomal compartments; d) high stability and nuclease resistance to protect oligonucleotide/oligonucleoside (OGN) cargos; e) lack of aggregation; and f) relatively neutral charge. It is noteworthy that several of these characteristics are key for avoiding immunotoxicity (32).

The TBG nanocapsule contains a 20-mer single-stranded chimeric OGN cargo designated as RNAi-CK2 and designed as a 14-mer DNA seed arm with a 6-mer RNA 3′ end. The sequence of this OGN is bi-specific in that it decreases expression of both CK2α and CK2α′ proteins. Importantly, in acute response HNSCC xenograft treatment studies, use of this TBG encapsulated OGN (TBG-RNAi-CK2) resulted in loss of CK2 expression, suppressed tumor growth, and changed survival and apoptosis-related gene expression consistent with the cell culture studies (23). Here we further elaborate on the use of the TBG nanocapsule to target CK2 in HNC, including data on the s50-TBG nanocapsule caveolar/lipid raft-mediated entry into cells and on the possible Ago2/RISC-mediated mechanism underlying the molecular targeting of CK2 in cancer cells. We have also delineated the biodistribution of s50-TBG nanocapsules using a xenograft cancer model in mice, and present data on the targeting of metastatic sites as well as on long-term survival in mice. Together, our data further underscore the therapeutic feasibility of RNAi molecular targeting of CK2 delivered via the cancer cell-specific s50-TBG nanocapsule.

Materials and Methods

Cell lines and culture

UM-SCC 11b tumor line was obtained from the University of Michigan squamous cell carcinoma series in 2000 (Ann Arbor, MI). The FaDu (HTB-43™) and SCC-15 (CRL-1623) tumor lines were purchased from ATCC in 2000 (Manassas, VA) and were cultured as per instructions from ATCC or as previously described (23); newly received cells were expanded, frozen back. Cells were cultured for less than 3 months per thaw. Cell lines were not authenticated by authors. Tissue culture plasticware and nanofibers (Corning) were coated with 0.5 μg/cm^2 of 2:1 (w/w) Tenascin-C (TNC, Millipore):Fibronectin-1 (FN1, Sigma-Aldrich) in 1X phosphate buffered saline (PBS). DOTAP (N-[1-(2,3-Dioleoyloxy)propyl]-N,N,N-trimethylammonium methyl-sulfate) transfection reagent

(Roche Applied Sciences) was used according to manufacturer's protocol. PEI-polyplexes (25 kDa PEI, Sigma-Aldrich) were prepared and used as described (33). Nanocapsule transfections were performed as described in Figs. 1–4 legends.

Immunoprecipitation analysis

Nuclear or cytosolic lysates were prepared as described (34), incubated for 3 h at 4° C with 200 nM of various fluorescein isothiocyanate (FITC)-labeled oligos then pulled down using "Catch and Release" columns (Millipore) with anti-FITC antibodies.

Western blot analysis

Western analysis was performed on whole cell, nuclear, and cytoplasmic lysates as described (20) using the following antibodies: CK2α, CK2α′ (Bethyl Laboratories A300-197A, A300-199A), caveolin-1, SP-3 (Santa Cruz Biotechnology sc-894, sc-644), Ago2 (Abnova 00027161), LDH (Cell Signaling 2012), Keratin-14 (Covance PRB155P), and FITC (Biodesign K9006G).

qRT-PCR analysis

For SYBR green quantitative reverse-transcriptase PCR (qRT-PCR), cDNA was transcribed from 0.5 μg of total RNA using Superscript III (Invitrogen). SYBR green reagents and huCK2α, huCK2α′ and (human glyceraldehyde 3-phosphate dehydrogenase) huGAPDH normalization primers were obtained from SABiociences, and used as described (25).

For endpoint PCR, total RNA was isolated from spleens using TRIzol Reagent (Invitrogen). Total RNA (0.5 μg) was used as template to perform RT-PCR using Titan One Tube™ RT-PCR system (Roche Molecular Diagnostics). Primers used were: 5'-GTTGCTTCCCGATACTTCAAAGG-3' (CK2α', F), 5'-GAACCTTGGCTATCCTCACCAAC-3' (CK2α', R), 171 bp product; 5'-TCCTCGTGGACTATCAGATG-3'(CK2α', F), 5'-AACCTTGGCAATGCGAAC-3' (CK2α', R) 140 bp product; 5'-CCCTTCATTGACCTCAAC-3' (GAPDH, F) 5'-TTCACACCCATCACAAAC-3' (GAPDH, R); 120 bp product. The PCR amplification included RT 50°C for 30 min, 94°°C for 4 min, 33 cycles of 94°°C, 45 sec; 55°C, 20 sec; 72°C, 45 sec with final 5 min extension at 72°C. For normalization, parallel RT-PCR reactions were performed with GAPDH primers using the same conditions. PCR products were separated by 1.0% agarose gel and stained with ethidium bromide. Images were acquired using a Kodak digital imaging system and quantitated using ImageJ.

Preparation of tenfibgen (TBG) nanocapsules

The sequences targeting CK2αα′ are shown in Fig. 1. FITC-labeled siRNAs and single-stranded oligos were modified at the 5' end. The TBG nanocapsules containing the oligos or green fluorescence protein (GFP) and luciferase reporter plasmids were manufactured as previously described (23, 35). Nanocapsules manufactured for *in vitro* use had bismuth tribromophenate added to the ligand shell to facilitate sedimentation and improve electron density.

Immunohistochemistry

Frozen sections were processed and antibodies used as described (25, 35). Other antibodies include GFP (Sigma G1544) and keratin-14 (Covance PRB155P). Nuclei were stained using Sytox Green (Life Technologies) or bisbenzamide. Images were acquired using Nikon C1si Laser Scanning Confocal Microscope.

Transmission Electron Microscopy

SCC-15 cells (2×10^5) were plated onto 4 well glass chambers coated with TNC:FN1 and treated with 2 μM TBG-siRNA. Following fixation and mounting, sections were lead-stained and examined using Phillips CM12 TEM microscope (45,000×).

Animals and HNSCC xenograft tumor models

Animals were housed in facilities approved by AAALAC in accordance with USDA, U.S. Department of HHS, and NIH. Experiments were conducted under approved IACUC protocols at University of Minnesota and MVAHCS. Balb/C athymic nude females (NCI) were used to generate the three xenograft models using intradermal flank inoculation with 4×10^6 FaDu, SCC-15 or UM-11b cells (23). Treatment amounts and regimens are described in legends for Figs. 4, 5 and Table 1. Tumors were measured using calipers and tumor volumes calculated by V = 0.5(L*W*W). At necropsy, blood, liver, kidney, spleen, lung, brain, primary and metastatic tumors were collected; portions of samples were embedded in OTC or flash frozen in liquid nitrogen for analysis. Blood and serum analysis was performed as described (35).

In vivo biodistribution

Balb/C athymic nude (NCI) female mice carrying FaDu tumors were treated (intravenous) i.v. with 3 mg/kg of TBG encapsulated iodine-derivatized siRNA when tumors were ~4–5 mm in diameter. Controls received TBG-trehalose (TBG-sugar) nanocapsules. At necropsy, blood and tissues were collected and shipped to the University of Missouri MURR facility for neutron activation analysis (NAA). By irradiation, tissue and siRNA iodine is converted to isotope I^{128} which allows for counting of gamma ray emission (36). Drug accumulation was calculated as the organ difference between animals receiving TBG-sugar and those receiving TBG-iodine-derivatized-siRNA nanocapsules.

Statistical Analysis

Percent of mice with tumor/metastases signal among those surviving the study were compared by treatment group using Fisher's Exact tests. Cell culture expression data, mouse spleen expression data, tumor and mouse weights were summarized and compared by treatment group for each tumor or sample type using analysis of variance (ANOVA). Means ± SD are presented. Overall survival, defined as time from treatment initiation to death or censorship at six (SCC-15, FaDu) or seven (UM-11b) months was summarized using Kaplan-Meier methods. Comparisons between the treatment and control groups were made using log rank tests. P-values for pairwise comparisons were conservatively adjusted for multiple comparisons using a Bonferroni correction and p-values <0.05 were considered statistically significant.

Results

Targeting CK2 using s50-TBG nanocapsules carrying RNAi molecules

We tested different chemistries of the same OGN sequence designed to target both the α and α´ catalytic subunits of CK2. This sequence is 100% complementary to the CK2α transcript, but has a single base mismatch with the CK2α´ mRNA. The various base modifications of these OGNs are presented in Fig. 1A. In order to facilitate nanocapsule uptake, FaDu cells were plated in 3D culture using 0.5 μg/cm^2 2:1 tenascin-C:fibronectin (TNC:FN1) -coated nanofiber scaffolds to improve cell surface lipid raft density. Treatment with TBG nanocapsule containing three types of OGN caused a varying level of reduction in the CK2α subunit ((RNAi-CK2 0.66 ± 0.15, siRNA to CK2αα´ (siCK2) 0.61 ± 0.08, antisense to CK2αα´ (AS-CK2) 0.84 ± 0.12)) (Fig. 1B). Several HNSCC cell lines were similarly cultured and treated with s50-TBG-RNAi-CK2 nanocapsules, and 48 h after treatment all five cancer cell lines demonstrated an inhibition of growth, with three cell lines showing statistically significant reduced growth (Fig. 1C). Corresponding analysis of the mRNA level by quantitative RT-PCR in cells treated with nanoencapsulated RNAi-CK2 showed a significant reduction in the α subunit transcript in FaDu cells detected 24 h after treatment (black bars compared with white bars, $p<0.05$; Fig. 1D); although CK2α´ mRNA was reduced it was not significantly different than the control sense-strand treated cells (white bars). Reductions in SCC-15 and UM-11b CK2α and α´ transcript levels were also modest.

Uptake of the s50-TBG nanocapsule is mediated via the caveolar/lipid raft pathway

To address the mechanism of entry of the s50-TBG nanocapsules into cancer cells, we utilized pharmacologic inhibitors of caveolar uptake (filipin and nystatin) or of endosomal uptake (bafilomycin) at varying concentrations. Fig. 2A illustrates representative results of the treatment of SCC-15 carcinoma cells with 2 μ g/ml of filipin prior to treatment of cells with 0.25 μ g/ml of s50-TBG-RNAi-CK2 (left panels) or 1.25 μ g/ml of FITC-labeled RNAi-CK2-PEI polyplexes (right top and middle panels). For this experiment, the s50-TBG nanocapsule shell was spiked with sheep IgG, and identified by using anti-sheep IgG (red signal). In Fig. 2A (left, top panel) the red signal denotes nuclear localization of the s50-TBG nanocapsules. Further, RNAi-CK2-PEI polyplexes were also directly visualized via the FITC label at the 5´ end of the RNAi-CK2 OGN (Fig. 2A right, top). Treatment with 2 μg/ml of filipin caused disappearance of the s50-TBG nuclear signal (Fig. 2A left, middle); however, the polyplexes continued to demonstrate a punctate distribution which was non-nuclear (Fig. 2A right, middle), consistent with the established uptake of PEI nucleic acid polyplexes by the endosomal pathway (37). Fig. 2B shows a representative transmission electron micrograph of s50-TBG nanocapsules in surface caveolae of SCC-15 cells grown on TNC:FN1 matrix and treated with 20 μM siCK2 encapsulated in s50-TBG nanocapsules. As shown in Fig. 2B, localization of s50-TBG nanocapsules is visualized in the caveolae. The micrograph also shows the trafficking of the nanocapsules along fibers consistent with cytoskeleton. Considering that the s50-TBG nanocapsules entered the cells via the caveolar/lipid raft pathway in cancer cells, we investigated if the matrix on which the cells grew affected expression of caveolin-1. Membrane-associated caveolin-1 protein levels were analyzed by immunoblot in HNSCC cell lines grown in 3D cultures on TNC:FN1 coated nanofiber scaffolds compared with standard tissue culture treated plastic plates; the results

demonstrated increased expression of caveolin-1 in hydrophobic membrane fractions of FaDu and UM-11b grown on TNC:FN1 scaffolds (Fig. 2C).

Delivery of single-stranded chimeric RNAi-CK2 via s50-TBG nanocapsules enhances Ago2 expression

Since Ago2 is the key Argonaute family protein responsible for cleaving the targeted transcript within small RNA-induced silencing complexes (RISCs) (38), we investigated whether or not Ago2 was involved in RNAi-CK2 induced reduction of CK2 expression. The results shown in Fig. 3A depict SCC-15 cells treated with 200 nM s50-TBG encapsulated FITC-labeled RNAi-CK2, DOTAP complexed FITC-labeled RNAi-CK2 or FITC-labeled siβ-gal, or no treatment control. Ago2 (red) and RNAi-CK2 (green) signals co-localize in the s50-TBG nanocapsule treated cells (top left) while this is not apparent in cells in which the single-stranded RNAi-CK2 OGN was delivered using DOTAP. As expected, the double-stranded siRNA, siβ–gal, signal also co-localized with Ago2. Fig. 3B shows analysis of Ago2 protein expression in SCC-15 cells treated with s50-TBG nanoencapsulated RNAi molecules compared with those introduced using DOTAP. The expression of the nuclear Ago2 was pronounced in the cells treated with s50-TBG encapsulated single-stranded RNAi and double-stranded siRNA molecules, while only the siRNA elicited significant nuclear Ago2 expression when introduced with DOTAP. No increase in cytosolic Ago2 expression was observed. A significant elevation of nuclear Ago2 was observed in response to s50-TBG nanoencapsulated OGN compared with corresponding controls ($p < 0.05$; Fig. 3B lower panel).

We next examined the interaction of Ago2 with RNAi-CK2 in SCC-15 cells 8, 24, and 36 h following treatment with s50-TBG nanoencapsulated FITC labeled RNAi-CK2. As shown in Fig. 3C, an increase in the perinuclear (8 and 36 h) and nuclear (24 h) co-localization of Ago2 (red) and FITC labeled RNAi-CK2 (green) was detected. To confirm the nuclear Ago2 loading of various siRNA and single-stranded RNAi molecules, and the importance of the growth environment in this process, SCC-15 cells grown on TNC:FN1-coated nanofiber scaffolds or standard tissue culture plastic were treated with s50-TBG nanocapsules containing FITC-labeled siRNAs or chimeric RNAi molecules. At 24 h post-treatment, the cells were harvested and fractionated for nuclear and cytosolic compartments using methodology in which endoplasmic reticulum remains associated with the nuclear fraction.. Western blot analysis of FITC-labeled OGNs immunoprecipitated with anti-FITC antibody indicated that Ago2 binds both siRNAs and the single-stranded RNAi structures and the Ago2/FITC-siRNA or RNAi complexes are primarily localized in the nuclear/nuclear-associated fraction (Fig. 3D). By comparison little OGN-associated nuclear Ago2 was detected in cells not grown on TNC:FN1-coated scaffolds, analogous to what was observed with caveolin-1 (Fig. 2C).

An analysis of the human HNC Affymetrix U-133a microarray database (39) indicated that Ago2 was significantly elevated in HNSCC compared with normal oral mucosa samples (Supplemental Fig. 1). Other genes relevant to the targeting/uptake of the s50-TBG nanocapsules by tumor cells such as tenascin C and caveolin-1 were also significantly upregulated. Among the putative receptors for tenascin-C (and TBG) are integrin α2 and

integrin β1; these genes are among those that showed the largest changes (62- and 234-fold increase, respectively) in the HNC tumors versus normal samples in this database (39).

Analysis of s50-TBG nanocapsule biodistribution in FaDu xenograft tumor bearing mice

To investigate the biodistribution of s50-TBG nanocapsules by neutron activation analysis, we produced TBG nanocapsules carrying an I^{127} derivatized siRNA cargo to administer to nude mice bearing FaDu flank xenograft tumors. Two hours after i.v. administration of the nanocapsules containing the I^{127}-siRNA or sugar (background control), the mice were sacrificed and collected tissues were subjected to neutron bombardment which converted I^{127} to I^{128}. The results on I^{128} gamma emissions were analyzed; Fig. 4A shows the cancer-cell specific uptake of the s50-TBG nanocapsules, with negligible amounts found in brain, kidney, liver and thyroid; these tissues were not saline perfused which may account for the presence of small amounts of the signal. Interestingly, the nanocapsule uptake appeared to be even more avid in the metastases (78% injected dose (ID)/g) compared with the primary tumor (18% ID/g).

Analysis of acute response to s50-TBG nanocapsule in FaDu metastatic spleen tumors

Using a cohort of 15 mice euthanized at day 3, we tested whether CK2 manipulation (by 1 × 25 mg/kg dose of the nanocapsules) was apparent in acutely-treated tumors and found that CK2 total protein levels were not altered by RNAi-CK2 treatment at day 3 (data not shown). Since CK2 shuttling from the nucleus precedes onset of apoptosis, we investigated post-treatment CK2 cellular distribution as well as the phosphorylation status of the CK2 substrate NFκB p65 using confocal microscopy. The result in Fig. 4B shows nuclear and cytoplasmic CK2 signal (green) in response to nanocapsules carrying sense control (top left), while treatment with nanoencapsulated RNAi-CK2 (top right) shows CK2 signal markedly affected in the nuclear compartment. The corresponding panels below depict the NF-κB p65 p-Ser529 signal (red) demonstrating that the RNAi-CK2 treatment dramatically affected the NF-κB status in the treated primary tumors (lower left).

We also analyzed the CK2 response in these same acutely treated FaDu xenograft mice which had developed metastases in the spleen. Immunoblot analysis for Keratin-14 and CK2αα′ in the primary tumor, naïve spleen, and tumor carrying spleen showed, CK2α and Keratin-14 levels were elevated in the tumor-bearing spleen and these proteins were down-regulated on treatment of the animals with TBG-RNAi-CK2 ($p=0.068$ and $p<0.0001$, respectively) relative to vehicle control (Fig. 4C). Quantitative RT-PCR analysis showed human-specific CK2α message was significantly down-regulated in splenic tumor compared to vehicle control in RNAi-CK2 treated animals (2.2±1.8 vs. 10.0±4.0; $p=0.012$). A significant reduction in CK2α′ mRNA levels was also observed between the RNAi-CK2 treatment and vehicle control (1.1±3.2 vs. 100.0±78.3; $p=0.066$).

To confirm our findings of a functional relationship between CK2 down-regulation and anti-tumor activity, we utilized confocal microscopy to compare naïve baseline spleen vs metastatic tumor-carrying spleen treated with s50-TBG-delivered reporter gene (nuclear-localized GFP), s50-TBG-RNAi-CK2, or vehicle. We found that Keratin-14-positive lesions were only GFP-positive in s50-TBG–GFP nanocapsule treated mice (Fig. 4D, pGFP versus

vehicle series). In contrast to vehicle treated animals, Keratin-14-positive lesions were not observed in s50-TBG-RNAi-CK2-treated or naïve spleen (Fig. 4D, B1 versus C1 and D1) consistent with the 13.9-fold reduction in Keratin-14 protein in the RNAi-CK2 treated animal's spleens (Fig 4C).

Finally, blood and serum analyses demonstrated no changes in hematological or blood chemistry profiles in these mice (Supplemental Tables 1 and 2).

Survival response of various HNSCC xenograft tumors to treatment with s50-TBG nanocapsules with RNAi-CK2 cargo

We investigated the survival response of several xenograft models of HNSCC using SCC-15, UM-11b and FaDu tumor cells treated with varying doses and regimens of s50-TBG-RNAi-CK2. CK2 and p53 expression characteristics in addition to other properties associated with aggressive tumors for the HNSCC models are summarized in Supplemental Table 3. The results in Fig. 5, panels A1, B1, and C1, show the tumor response to varying doses of TBG-RNAi-CK2. Tumor bearing animals treated with one or two doses of the drug demonstrated a persistent reduction in tumor volume 35 days after treatment initiation. Moreover, significantly improved survival was observed compared to control groups up to 200 days following treatment; notably, 25 of 46 animals survived without any local recurrence. In contrast, only 12 of the 53 control animals from the 3 study groups survived. No control animals carrying FaDu tumor lived beyond 50 days, and only 2 animals carrying SCC-15 tumors lived past 150 days. Further, treated flank tumors resolved by a wound healing process subsequent to vessel hemorrhage (which resembled bruising) rather than a conventional "shrinking". There was no significant change in the animal weights over the course of the study (Supplemental Fig. 2).

Information on tumor burden in the surviving mice in relation to dose level and therapy regimen is shown in Table 1. At the end of the survival period, all remaining animals were treated with s50-TBG nanocapsules containing a luciferase expressing plasmid to determine in vivo tumor burden in primary and metastatic sites (10). The results indicate that of the 25 surviving s50-TBG-RNAi-CK2 treated animals the percentage with any metastatic tumor burden ranged from 33% (UM-11b, 3 of 9; FaDu, 2 of 6) to 10% (SCC-15, 1 of 10). In contrast, of the remaining 12 sense-RNAi and vehicle treated control mice (UM-11b, 10; SCC-15, 2), all but 1 (i.e., 92%) had detectable local and metastatic tumors.

Discussion

In recent years, considerable progress has been made towards developing cancer therapies that are designed to target specific deregulated pathways or molecules. Indeed, these targets may represent one or more hallmarks of cancer (40). However, fundamental concerns pertaining to such therapies remain. First, lack of drug delivery in a cancer cell specific manner may have potent side-effects and considerable toxicity in the host. Second, even when therapeutic effects are noted they tend to be transient with re-emergence of the cancer due not only to the development of drug resistance pathways but also to the possible ever-changing reliance of cancer cells on alternate pathways and molecules for survival (40). Ideally, for effective cancer therapy the target should be unique to malignancy and without

redundancy in the cell so that its targeting results in specific cancer cell death. However, such a situation is now considered highly unlikely for the majority of cancers.

Protein kinase CK2 has been found to be elevated in all cancers that have been examined (6, 10). This increase in CK2 expression correlates with increased nuclear localization, is not associated with any mutational changes in CK2 genes, and serves as a prognostic indicator (5, 9). Its role in cancer cell biology likely relates to its interaction with various hallmarks of cancer (7, 40, 41), and we originally proposed CK2 as a potentially important target for cancer therapy (14). Since then, much evidence has come forth to support CK2 as a druggable target (20, 21, 42). Certainly, while a “pharmacological window” may exist for targeting of CK2 since normal/benign cells tend to be relatively resistant to downregulation of CK2, its cancer cell specific targeting would be highly desirable (14). To that end, we have designed a novel nanocapsule that can deliver its cargo specifically to target CK2 in cancer cells while avoiding the normal cells (7, 10,16,23–25, 43).

Our results on the mechanism by which s50-TBG nanocapsules enter the cell demonstrate the involvement of the caveolar/lipid raft pathway, providing a mechanism for avoiding the endosomal pathway and preventing activation of the innate immune response (44, 45). This relates to the sub-50 nm size of the TBG encapsulated RNAi-CK2, which unlike conventional liposomes or other nanoparticle delivery strategies is below the known size exclusion for the lipid raft/caveolar pathway. Our data also suggest the importance of the cancer cell environment for drug uptake and processing. In the case of cultured cells, this translated to the necessity for growing cells on an extracellular matrix support containing tenascin-C and fibronectin. The extracellular protein-enriched scaffolds allowed for increased Ago2 expression and association with the OGN drug cargo in the nuclear and nuclear-associated fractions upon treatment with TBG encapsulated OGN; consistent with Ago2 association with single-stranded small RNAs in the nucleus and Ago2 localization to the perinuclear region (46, 47); whereas growth of cells on plastic was not favorable for OGN/Ago2 association. This suggests targeting of CK2αα' mRNAs via the nanoencapsulated RNAi-CK2 is achieved, at least in part, through the Ago2/RISC pathway. Further, it is possible that the s50 TBG nanocapsule may enhance RNAi efficacy in the cell by delivering the OGN specifically to nuclear and nuclear-associated Ago2 locations (48). Of note, all three xenograft models responded to RNAi-CK2 treatment with significantly improved survival, and remained free of local recurrence for 6 months, despite variances in their basal Ago2 expression levels. As we achieved significant reduction in vivo of orthotopic prostate xenografts using naked phosphorothioate antisense DNA with the identical bi-specific sequence targeting CK2, it suggests that the chimeric DNA/RNA hybrid used in the current study might also target the CK2αα' transcripts for destruction via RNase H (18).

We propose that the malignant cell specificity of the s50-TBG nanocapsule is achieved by the nature of the protein which forms the shell of the nanocapsule, namely TBG. The receptors for tenascin-C are known to be elevated in cancer cells including HNSCC, while these receptors are minimal in normal cells (29, 31, 49). Human and mouse TBG peptides are 93% perfectly identical and 99% positively identical taking into account conservative amino acid changes, thus the TBG nanocapsule is predicted to elicit the same biological

activities in tissues of mouse and human origin. Our data also provide further evidence that s50-TBG nanocapsules target cancer cells and not the normal cells —specifically, biodistribution data demonstrate that the OGN drug cargo accumulation is much greater in primary and especially metastatic lymph node tumor tissue as compared to non-tumor tissues such as liver and spleen, thereby avoiding preferential accumulation in the RES.

We previously demonstrated that s50-TBG-RNAi-CK2 was effective in acute HNSCC response studies at reducing tumor growth and inducing changes in tumor cell signaling anticipated for treatment response (23). Here, using higher s50-TBG-RNAi-CK2 dosing levels in which survival out to 6 months was examined, we have noted that the xenograft tumor response is remarkably sensitive to the dose level and regimen of therapy treatment. Dose response analysis of survival data at the highest doses is confounded due to frequent occurrence of rapid tumor death response and, in some cases, subsequent animal death. Such a response was the most pronounced in the FaDu xenograft as it was observed at single doses ≥ 10 mg/kg. Interestingly, these tumors also expressed the highest levels of Ago2 among the three cell lines used in our studies. UM-11B showed moderate rapid tumor death response, and also expressed the second-highest levels of Ago2. The rapid form of tumor death response was minimal in the SCC-15 model, which had the lowest Ago2 levels.

Remarkably, our data demonstrate the ability of s50-TBG-RNAi-CK2 to target metastatic spleen and elicit a response by shutting down CK2 expression. Although an approximate 2-fold reduction in CK2α transcript was observed with the sense-RNAi-CK2 control in the splenic metastases, little change in the cytosolic or nuclear CK2αα′ protein levels was observed. An analysis of sense-RNAi-CK2 sequence by Biobridge indicated it could act as an anti-CK2α but not anti-CK2α′ sequence. In contrast, the bi-specific RNAi-CK2 reduced the transcripts and protein levels in all cellular compartments and for both subunits by at least 65%. As the sense-RNAi-CK2 provided no survival advantage, these results support the importance of targeting both kinase subunits of the enzyme to achieve effective cancer cell killing. Furthermore, it is particularly noteworthy that the efficacy of the TBG-RNAi-CK2 treatment was observed regardless of cellular p53 mutational status or of EGFR expression. Together, these results indicate that s50-TBG encapsulated RNAi-CK2 is delivered specifically to primary and metastatic tumors in a wide range of HNSCCs; is effective in downregulating CK2; and achieves significant tumor-free survival following only a two dose therapy regimen.

In summary, we have demonstrated that s50-TBG nanocapsules carrying RNAi-CK2 administered for brief periods of time at relatively low doses target cancer cells specifically in both primary and metastatic tumors without affecting the normal cells, thereby serving as an effective therapeutic for several xenograft HNSCC tumor models, and resulting in significant post-treatment survival of the tumor bearing mice. This suggests that the combined impacts of targeting CK2 with the nanocapsule’s ability to affect metastases fulfill an important deficit in current nanoparticle drug strategies (50).

Supplementary Material

Refer to Web version on PubMed Central for supplementary material.

Acknowledgments

We thank Diane K. Tobolt for her assistance in the laboratory. Nikon confocal images were acquired using the facilities of the University Imaging Centers at the University of Minnesota.

Financial Information: This work is supported in part by merit review research funds (1IO1B001831) awarded by the Department of Veterans Affairs (K. Ahmed), research grant CA150182 awarded by National Cancer Institute, NIH, Department of Health and Human Services (K. Ahmed), research grants CA158730 and DK067436-05 awarded by NCI and NIDDK, respectively, NIH, Department of Health and Human Services (B.T. Kren), research grants HHS-N261-2008-00027/N42CM-2008-00027C, CA99366, and CA119556 awarded by National Cancer Institute, NIH, Department of Health and Human Services (G.M. Unger).

List of abbreviations

Ago2	argonaute 2
CK2	official acronym for former casein kinase 2 or II
DOTAP	N-[1-(2,3-Dioleoyloxy)propyl]-N,N,N-trimethylammonium methyl-sulfate
FBS	fetal bovine serum
FITC	fluorescein isothiocyanate
β-gal	β-galactosidase
GAPDH	glyceraldehyde 3-phosphate dehydrogenase
GFP	green fluorescence protein
HNC	head and neck cancer
HNSCC	head and neck squamous cell carcinoma
i.v.	intravenous
ID	injected dose
OGN	oligonucleotide or oligonucleoside
PBS	phosphate buffered saline
PCR	polymerase chain reaction
PCa	prostate cancer
Q-RT-PCR	quantitative reverse-transcriptase PCR
RNAi	RNA interference
siCK2	siRNA to CK2αα′
siRNA	small interfering RNA
s50 or sub-50 nm	less than 50 nm in size
TBG	tenfibgen (the carboxy terminal fibrinogen globe domain of tenascin-C or TN-C)
TNC:FN1	tenascin-C and fibronectin 1 in 2:1 ratio

References

1. Society AC. Cancer Facts & Figures 2014. 2014 Available from: http://wwwcancerorg/acs/groups/content/@research/documents/webcontent/acspc-042151pdf.
2. Leemans CR, Braakhuis BJ, Brakenhoff RH. The molecular biology of head and neck cancer. Nature reviews Cancer. 2011; 11:9–22.
3. Chaturvedi AK, Engels EA, Pfeiffer RM, Hernandez BY, Xiao W, Kim E, et al. Human papillomavirus and rising oropharyngeal cancer incidence in the United States. Journal of clinical oncology : official journal of the American Society of Clinical Oncology. 2011; 29:4294–4301. [PubMed: 21969503]
4. Vermorken JB, Guigay J, Mesia R, Trigo JM, Keilholz U, Kerber A, et al. Phase I/II trial of cilengitide with cetuximab, cisplatin and 5-fluorouracil in recurrent and/or metastatic squamous cell cancer of the head and neck: findings of the phase I part. British journal of cancer. 2011; 104:1691–1696. [PubMed: 21540865]
5. Guerra B, Issinger OG. Protein kinase CK2 in human diseases. Curr Med Chem. 2008; 15:1870–1886. [PubMed: 18691045]
6. Ruzzene M, Pinna LA. Addiction to protein kinase CK2: a common denominator of diverse cancer cells? Biochim Biophys Acta. 2010; 1804:499–504. [PubMed: 19665589]
7. Trembley JH, Wang G, Unger G, Slaton J, Ahmed K. Protein kinase CK2 in health and disease: CK2: a key player in cancer biology. Cell Mol Life Sci. 2009; 66:1858–1867. [PubMed: 19387548]
8. Gapany M, Faust RA, Tawfic S, Davis A, Adams GL, Ahmed K. Association of elevated protein kinase CK2 activity with aggressive behavior of squamous cell carcinoma of the head and neck. Mol Med. 1995; 1:659–666. [PubMed: 8529132]
9. Tawfic S, Yu S, Wang H, Faust R, Davis A, Ahmed K. Protein kinase CK2 signal in neoplasia. Histol Histopathol. 2001; 16:573–582. [PubMed: 11332713]
10. Trembley JH, Chen Z, Unger G, Slaton J, Kren BT, Van Waes C, et al. Emergence of protein kinase CK2 as a key target in cancer therapy. BioFactors. 2010; 36:187–195. [PubMed: 20533398]
11. Guo C, Yu S, Davis AT, Wang H, Green JE, Ahmed K. A potential role of nuclear matrix-associated protein kinase CK2 in protection against drug-induced apoptosis in cancer cells. J Biol Chem. 2001; 276:5992–5999. [PubMed: 11069898]
12. Ahmed K, Gerber DA, Cochet C. Joining the cell survival squad: an emerging role for protein kinase CK2. Trends Cell Biol. 2002; 12:226–230. [PubMed: 12062170]
13. Faust RA, Tawfic S, Davis AT, Bubash LA, Ahmed K. Antisense oligonucleotides against protein kinase CK2-α inhibit growth of squamous cell carcinoma of the head and neck *in vitro*. Head Neck. 2000; 22:341–346. [PubMed: 10862016]
14. Wang H, Davis A, Yu S, Ahmed K. Response of cancer cells to molecular interruption of the CK2 signal. Mol Cell Biochem. 2001; 227:167–174. [PubMed: 11827168]
15. Unger GM, Davis AT, Slaton JW, Ahmed K. Protein kinase CK2 as regulator of cell survival: implications for cancer therapy. Curr Cancer Drug Targets. 2004; 4:77–84. [PubMed: 14965269]
16. Wang G, Unger G, Ahmad KA, Slaton JW, Ahmed K. Downregulation of CK2 induces apoptosis in cancer cells--a potential approach to cancer therapy. Mol Cell Biochem. 2005; 274:77–84. [PubMed: 16342410]
17. Slaton JW, Unger GM, Sloper DT, Davis AT, Ahmed K. Induction of apoptosis by antisense CK2 in human prostate cancer xenograft model. Mol Cancer Res. 2004; 2:712–721. [PubMed: 15634760]
18. Trembley JH, Unger GM, Tobolt DK, Korman VL, Wang G, Ahmad KA, et al. Systemic administration of antisense oligonucleotides simultaneously targeting CK2alpha and alpha' subunits reduces orthotopic xenograft prostate tumors in mice. Mol Cell Biochem. 2011; 356:21–35. [PubMed: 21761204]
19. Prudent R, Moucadel V, Lopez-Ramos M, Aci S, Laudet B, Mouawad L, et al. Expanding the chemical diversity of CK2 inhibitors. Mol Cell Biochem. 2008; 316:71–85. [PubMed: 18563535]
20. Pagano MA, Bain J, Kazimierczuk Z, Sarno S, Ruzzene M, Di Maira G, et al. The selectivity of inhibitors of protein kinase CK2: an update. Biochem J. 2008; 415:353–365. [PubMed: 18588507]

21. Siddiqui-Jain A, Drygin D, Streiner N, Chua P, Pierre F, O'Brien SE, et al. CX-4945, an Orally Bioavailable Selective Inhibitor of Protein Kinase CK2, Inhibits Prosurvival and Angiogenic Signaling and Exhibits Antitumor Efficacy. Cancer Research. 2010; 70:10288–10298. [PubMed: 21159648]
22. Faust RA, Niehans G, Gapany M, Hoistad D, Knapp D, Cherwitz D, et al. Subcellular immunolocalization of protein kinase CK2 in normal and carcinoma cells. Int J Biochem Cell Biol. 1999; 31:941–949. [PubMed: 10533285]
23. Brown MS, Diallo OT, Hu M, Ehsanian R, Yang X, Arun P, et al. CK2 Modulation of NF-κB, TP53, and the Malignant Phenotype in Head and Neck Cancer by Anti-CK2 Oligonucleotides In vitro or In vivo via Sub–50-nm Nanocapsules. Clin Cancer Res. 2010; 16:2295–2307. [PubMed: 20371694]
24. Unger, G.; Trembley, J.; Kren, B.; Ahmed, K. Nanoparticles in Cancer Therapy. In: Schwab, M., editor. Encyclopedia of Cancer: Springer Reference. Springer-Verlag Berlin Heidelberg: 2012. p. 1-4.(wwwspringerreferencecom). 2009 [Jan 31, 2012]
25. Trembley JH, Unger GM, Korman VL, Tobolt DK, Kazimierczuk Z, Pinna LA, et al. Nanoencapsulated anti-CK2 small molecule drug or siRNA specifically targets malignant cancer but not benign cells. Cancer Letters. 2012; 315:48–58. [PubMed: 22050909]
26. Erickson HP, Bourdon MA. Tenascin: an extracellular matrix protein prominent in specialized embryonic tissues and tumors. Annu Rev Cell Biol. 1989; 5:71–92. [PubMed: 2480799]
27. Aukhil I, Joshi P, Yan Y, Erickson HP. Cell- and heparin-binding domains of the hexabrachion arm identified by tenascin expression proteins. J Biol Chem. 1993; 268:2542–2553. [PubMed: 7679097]
28. Yokoyama K, Erickson HP, Ikeda Y, Takada Y. Identification of amino acid sequences in fibrinogen gamma -chain and tenascin C C-terminal domains critical for binding to integrin alpha vbeta 3. J Biol Chem. 2000; 275:16891–16898. [PubMed: 10747940]
29. Desgrosellier JS, Cheresh DA. Integrins in cancer: biological implications and therapeutic opportunities. Nature reviews Cancer. 2010; 10:9–22.
30. Oskarsson T, Acharyya S, Zhang XH, Vanharanta S, Tavazoie SF, Morris PG, et al. Breast cancer cells produce tenascin C as a metastatic niche component to colonize the lungs. Nat Med. 2011; 17:867–874. [PubMed: 21706029]
31. Van Obberghen-Schilling E, Tucker RP, Saupe F, Gasser I, Cseh B, Orend G. Fibronectin and tenascin-C: accomplices in vascular morphogenesis during development and tumor growth. Int J Dev Biol. 2011; 55:511–525. [PubMed: 21769776]
32. Schellekens H. Factors influencing the immunogenicity of therapeutic proteins. Nephrol Dial Transplant. 2005; 20(Suppl 6):vi3–vi9. [PubMed: 15958824]
33. Boussif O, Lezoualc'h F, Zanta MA, Mergny MD, Scherman D, Demeneix B, et al. A versatile vector for gene and oligonucleotide transfer into cells in culture and in vivo: polyethylenimine. Proc Natl Acad Sci U S A. 1995; 92:7297–7301. [PubMed: 7638184]
34. Weinberg MS, Villeneuve LM, Ehsani A, Amarzguioui M, Aagaard L, Chen ZX, et al. The antisense strand of small interfering RNAs directs histone methylation and transcriptional gene silencing in human cells. RNA. 2006; 12:256–262. [PubMed: 16373483]
35. Kren BT, Unger GM, Sjeklocha L, Trossen AA, Korman V, Diethelm-Okita BM, et al. Nanocapsule-delivered *Sleeping Beauty* mediates therapeutic Factor VIII expression in liver sinusoidal endothelial cells of hemophilia A mice. J Clin Invest. 2009; 119:2086–2099. [PubMed: 19509468]
36. Mason M, Spate V, Morris J, Baskett C, Cheng T, Reams C, et al. Determination of iodine in urine, using epithermal instrumental neutron activation analysis (EINAA), at the University of Missouri Research Reactor (MURR). Journal of Radioanalytical and Nuclear Chemistry. 1995; 195:57–65.
37. Varga CM, Tedford NC, Thomas M, Klibanov AM, Griffith LG, Lauffenburger DA. Quantitative comparison of polyethylenimine formulations and adenoviral vectors in terms of intracellular gene delivery processes. Gene Ther. 2005; 12:1023–1032. [PubMed: 15815703]
38. Meister G, Landthaler M, Patkaniowska A, Dorsett Y, Teng G, Tuschl T. Human Argonaute2 mediates RNA cleavage targeted by miRNAs and siRNAs. Mol Cell. 2004; 15:185–197. [PubMed: 15260970]

39. Ginos M, Page G, Michalowicz B, Patel K, Volker S, Pambuccian S, et al. Identification of a gene expression signature associated with recurrent disease in squamous cell carcinoma of the head and neck. Can Res. 2004; 64:55–63.
40. Hanahan D, Weinberg RA. Hallmarks of cancer: the next generation. Cell. 2011; 144:646–674. [PubMed: 21376230]
41. Trembley, JH.; Wu, J-J.; Unger, GM.; Kren, BT.; Ahmed, K. CK2 Suppression of Apoptosis and Its Implication in Cancer Biology and Therapy. In: Pinna, LA., editor. Protein Kinase CK2. First ed.. Oxford: John Wiley & Sons, Inc.; 2013. p. 319-343.
42. Sarno S, Papinutto E, Franchin C, Bain J, Elliott M, Meggio F, et al. ATP site-directed inhibitors of protein kinase CK2: an update. Curr Top Med Chem. 2011; 11:1340–1351. [PubMed: 21513497]
43. Ahmad KA, Wang G, Slaton J, Unger G, Ahmed K. Targeting CK2 for cancer therapy. Anticancer Drugs. 2005; 16:1037–1043. [PubMed: 16222144]
44. Sioud M. Induction of inflammatory cytokines and interferon responses by double-stranded and single-stranded siRNAs is sequence-dependent and requires endosomal localization. Journal of molecular biology. 2005; 348:1079–1090. [PubMed: 15854645]
45. Szebeni J, Moghimi SM. Liposome triggering of innate immune responses: a perspective on benefits and adverse reactions. J Liposome Res. 2009; 19:85–90. [PubMed: 19514998]
46. Gagnon KT, Li L, Chu Y, Janowski BA, Corey DR. RNAi Factors Are Present and Active in Human Cell Nuclei. Cell Rep. 2014; 6:211–221. [PubMed: 24388755]
47. Stalder L, Heusermann W, Sokol L, Trojer D, Wirz J, Hean J, et al. The rough endoplasmatic reticulum is a central nucleation site of siRNA-mediated RNA silencing. EMBO J. 2013; 32:1115–1127. [PubMed: 23511973]
48. Nguyen J, Szoka FC. Nucleic acid delivery: the missing pieces of the puzzle? Acc Chem Res. 2012; 45:1153–1162. [PubMed: 22428908]
49. Tuxhorn JA, Ayala GE, Smith MJ, Smith VC, Dang TD, Rowley DR. Reactive Stroma in Human Prostate Cancer. Clinical Cancer Research. 2002; 8:2912–2923. [PubMed: 12231536]
50. Schroeder A, Heller DA, Winslow MM, Dahlman JE, Pratt GW, Langer R, et al. Treating metastatic cancer with nanotechnology. Nat Rev Cancer. 2012; 12:39–50. [PubMed: 22193407]

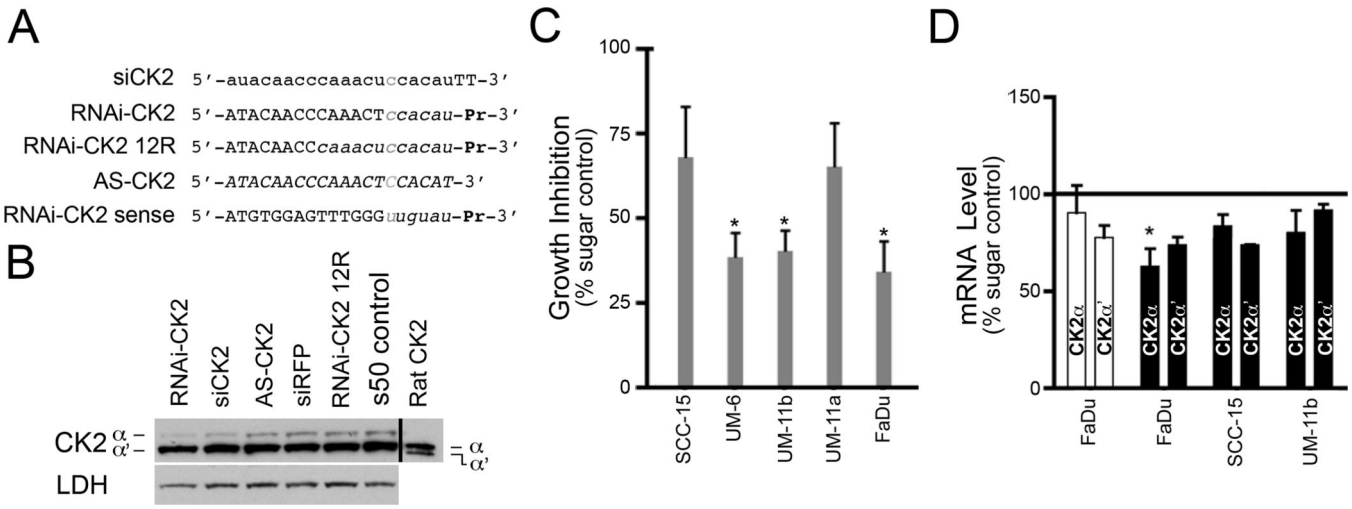

Figure 1.

s50-TBG nanoencapsulated RNAi targets both α and α′ subunits of CK2 in HNCC lines *in vitro*. A, sequence and chemical modifications of the OGN. DNA residues are uppercase and italics indicating phosphorothioate linkages; RNA residues are lowercase with italics indicating 2′-*O*-methyl modified RNA residues. The single base mismatch between the OGN used and the CK2α′ subunit mRNA is shown in grey. The 3′ overhanging bases of the siRNA and the 3′ propyl modifications of the single-stranded OGN are indicated by TT and **Pr**, respectively. B, immunoblot showing the effect on CK2α and α′ subunits 72 h after addition of 15 μM s50-TBG nanocapsules containing RNAi-CK2 with 6 RNA residues (RNAi-CK2), siCK2, RNAi-CK2 with 12 RNA residues (RNAi-CK2-12R), sugar (s50 control), phosphorothioate antisense (AS-CK2), or siRNA targeting red fluorescent protein (siRFP). CK2 purified from rat liver was used as a positive control. Lactate dehydrogenase (LDH) was used as a loading control. C, growth inhibition of human HNSCC lines was determined by [^{3}H]-thymidine incorporation 48 h after treatment with 20 μM s50-TBG-RNAi-CK2 vs s50-TBG-sugar. Mean ± SE are shown. *$p<0.002$ D, mRNA levels of CK2α and CK2α′ were determined by SYBR green quantitative RT-PCR 24 h after treatment with 20 μM s50-TBG-RNAi-CK2 (black bars) or the CK2 sense-RNAi control (white bars). Levels were normalized using GAPDH transcript and are expressed relative to 20 μM s50-TBG-sugar treated cells. Mean ± SE are shown. *$p<0.05$.

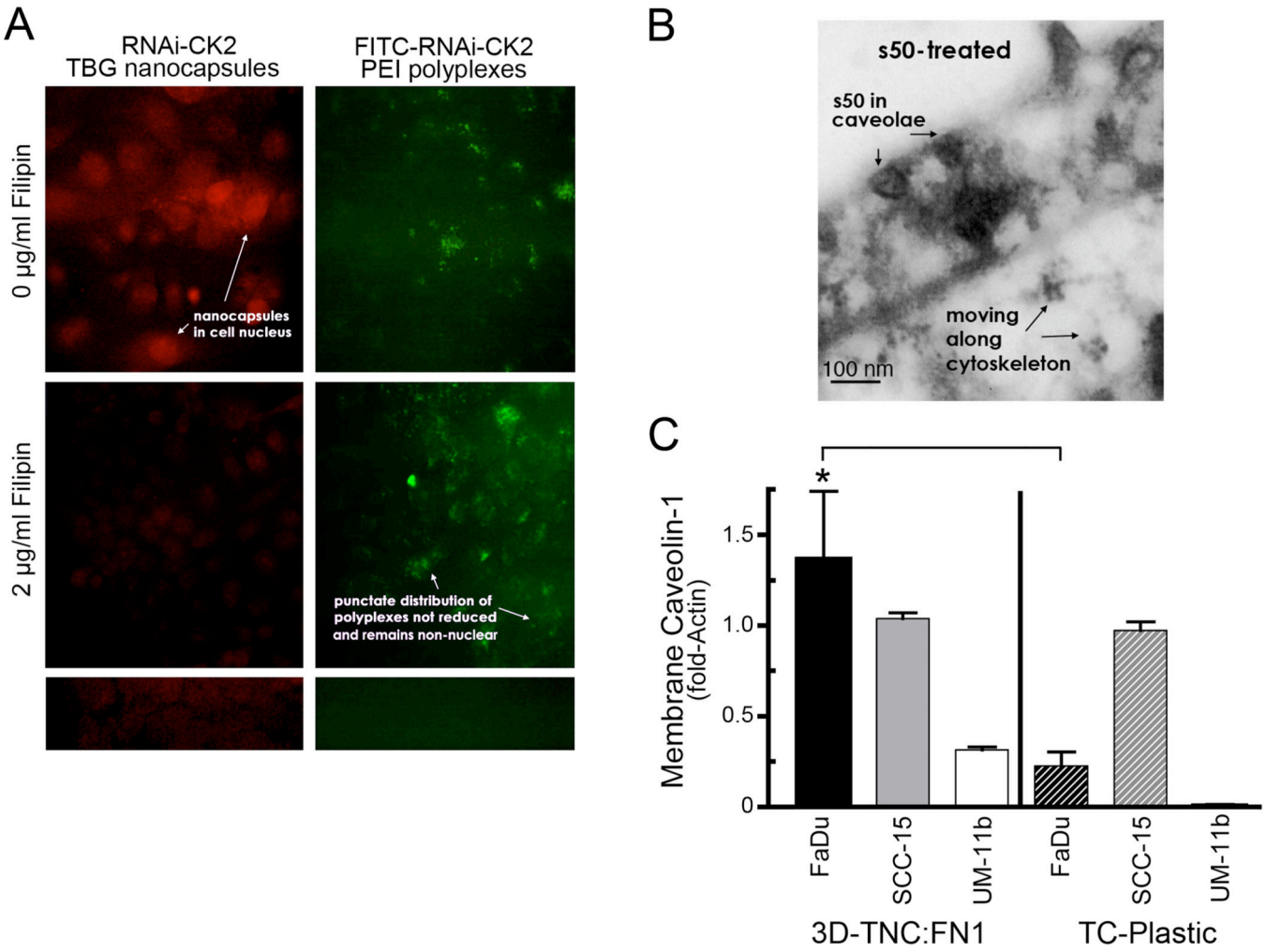

Figure 2.

Uptake of the s50-TBG nanocapsule is mediated *via* caveolae/lipid raft pathway. A, SCC-15 cells were first treated with 2 µg/ml filipin to disrupt caveolae (middle panels), then with 1 µg/ml s50-TBG-RNAi-CK2 (left panels) or 5 µg/ml FITC-labeled RNAi-CK2-PEI polyplexes (right, top and middle). Nanocapsules (red) were indirectly detected by fluorescent anti-sheep IgG (left, top and middle). RNAi-CK2-PEI polyplexes were directly visualized via the FITC-label (right). No-primary antibody control is shown at bottom left and untreated control at bottom right. Original magnification, 40,000×. B, transmission electron micrograph of nanocapsules in surface caveolae of SCC-15 cells grown on TNC:FN1 and treated with 20 µM s50-TBG-siCK2. Original magnification, 45,000×. C, membrane-associated caveolin-1 expression is upregulated in HNSCC lines grown on TNC:FN1 coated nanofibers versus standard tissue culture (TC) plasticware. Mean ± SE are shown. *$p<0.0001$.

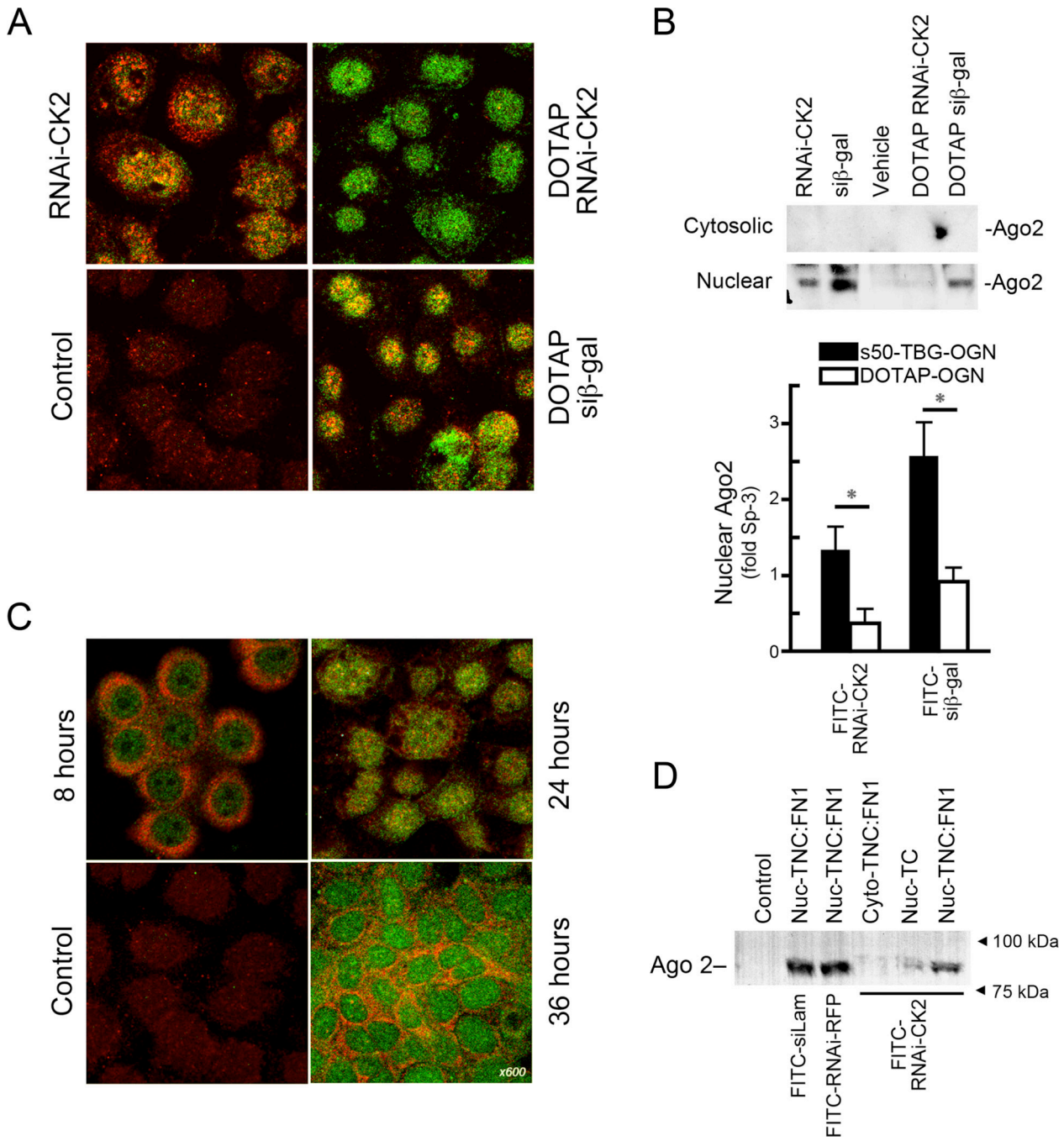

Figure 3.

s50-TBG nanoencapsulation enhances Ago2 expression and loading of single-stranded chimeric RNAi molecules. A, SCC-15 cells plated on TNC:FN1 24 h after treatment with 200 nM TBG-FITC-RNAi-CK2, DOTAP complexed FITC-RNAi-CK2 or FITC-siβ-gal, or no treatment control (Control). FITC-labeled OGN are green and Ago2 proteins are red. B, immunoblots showing the nuclear localization of Ago2 in SCC-15 cells plated on TNC:FN1 treated with 200 nM s50-TBG-FITC-RNAi-CK2 (RNAi-CK2) or s50-TBG-FITC-siβ-gal (siβ-gal); vehicle treated control (Vehicle); DOTAP complexed FITC-RNAi-CK2 (DOTAP

RNAi-CK2) or FITC-siβ-gal (DOTAP siβ-gal). Quantitation of nuclear Ago2 normalized to Sp-3 and relative to respective vehicle controls is shown (Mean ± SE). *$p<0.05$. C, time course of FITC-RNAi-CK2 interaction with Ago2 following treatment of SCC-15 cells plated on TNC:FN1 with 200 nM s50-TBG-FITC-RNAi-CK2. FITC-labeled OGN (green), Ago2 proteins (red), and co-localized Ago2:FITC-OGN (yellow) are shown in merged images. D, immunoblot confirmation of nuclear Ago2 loading of FITC-RNAi-CK2 (RNAi-CK2), FITC-anti-red fluorescent protein-RNAi (RNAi-RFP) or FITC-siLaminin (siLam). Nuclear or cytosolic lysates from SCC-15 cells grown on TNC:FN1 nanofiber scaffolds or tissue culture plasticware were incubated with the different FITC-labeled OGN, immunoprecipitated with anti-FITC antibodies, and subjected to immunoblot analysis using anti-Ago2 antibody. Goat serum control (Control); SCC-15 nuclear lysates from TNC:FN1 nanofiber grown cells (Nuc-TNC:FN1); cytosolic extract from TNC:FN1 nanofiber grown cells (Cyto-TNC:FN1); nuclear lysate from untreated tissue culture plastic grown SCC-15 cells (Nuc-TC).

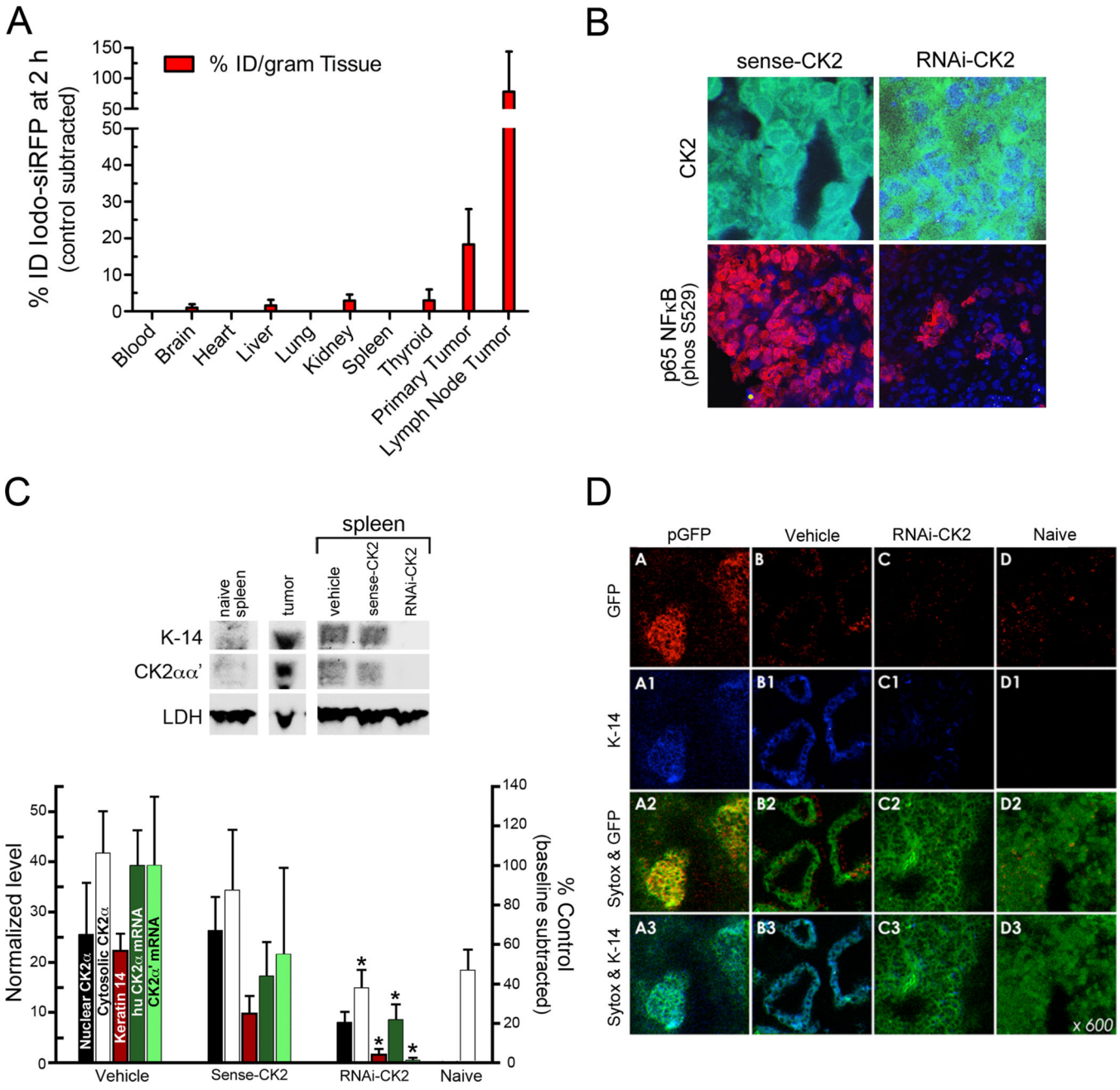

Figure 4.

Biodistribution and acute efficacy of s50-TBG nanocapsules in FaDu tumor xenograft mice. A, biodistribution was determined in vivo 2 h after i.v. administration of s50-TBG nanocapsules containing I^{127}-siRNA to nude mice bearing FaDu tumors (n=3) by neutron activation analysis of the tissues. Levels of endogenous tissue iodine were measured in FaDu tumor mice treated with s50-TBG-sugar (n=2). The results are expressed as % injected dose (ID) per gram of tissue. B, acute effects in primary tumor after i.v. administration of 25 mg/kg s50-TBG-RNAi-CK2 in FaDu xenograft mice. Cryosections were labeled with anti-CK2 (green) or anti-NFκB p65 p-Ser 529 (red). Nuclei (blue) were counterstained with

bisbenzamide. C, immunoblot showing the inhibition of CK2 expression in FaDu xenograft metastatic spleens 3 days after i.v. administration of 25 mg/kg s50-TBG-RNAi-CK2. Densitometric analysis of the immunoblots is depicted. Nuclear CK2α (white) protein is normalized to Sp-3; cytosolic CK2α (black) and keratin-14 (K-14, red) proteins are normalized to LDH. End-point qRT-PCR analysis crossing the predicted cleavage site targeted in the human CK2α (dark green) and CK2α′ (light green) transcripts in the tumor burdened FaDu spleens is also graphed. Transcript values were normalized to GAPDH and the endogenous naïve mouse spleen baseline transcript values for CK2α′ were subtracted. The data shown are mean ± SE from 5 animals per group. *P values are given under results. D, confocal micrographs confirming the co-localization of K-14 and FaDu tumor and the efficacy of s50-TBG-RNAi-CK2 in reducing spleen metastases. Single signals are K-14 (blue) and GFP (red). DNA was counterstained with Sytox Green. Merged signals are GFP and Sytox Green (yellow), and K-14 and Sytox Green (cyan).

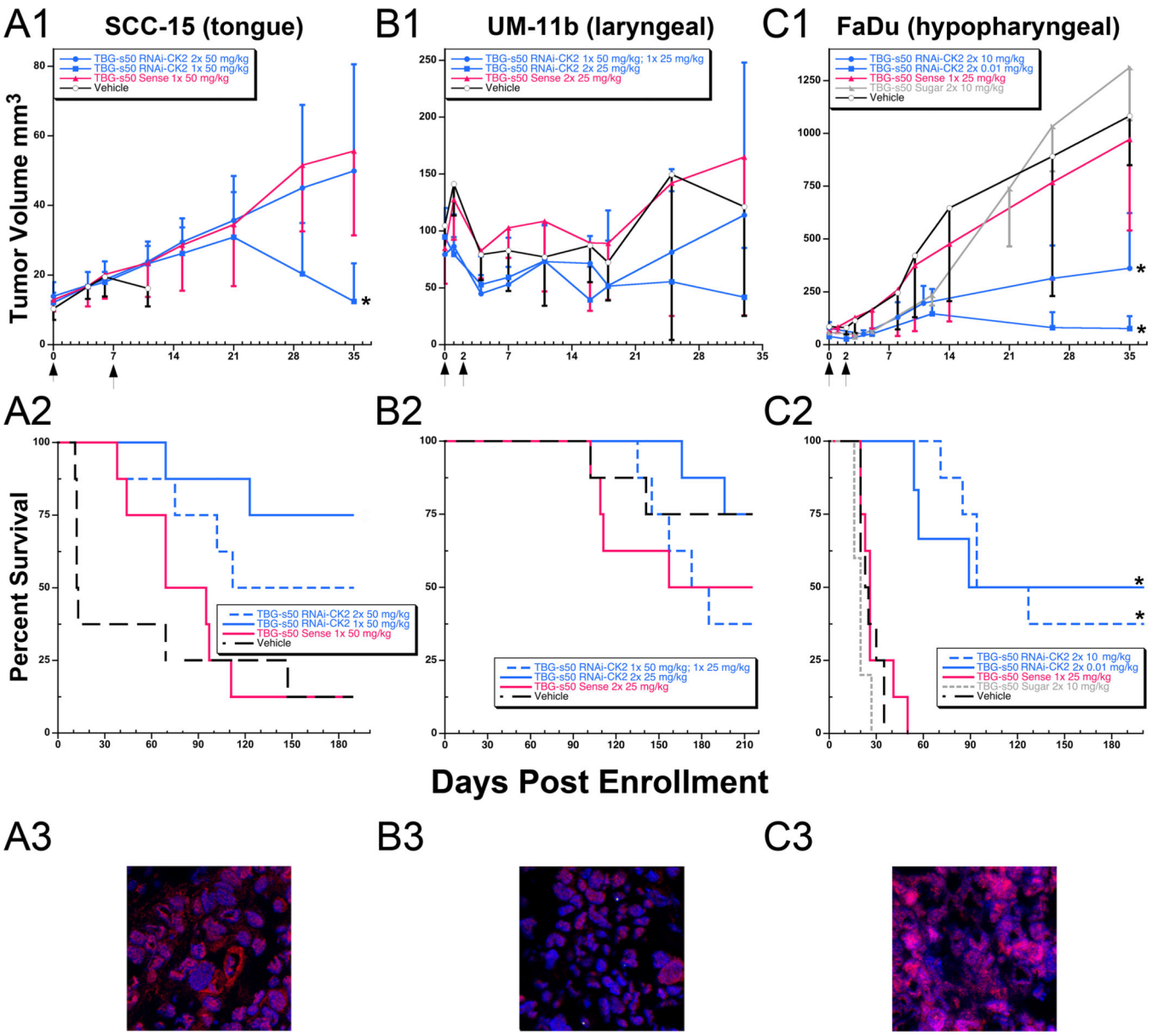

Figure 5.

Tumor volume and survival in SCC-15, UM-11b and FaDu HNSCC xenograft tumor models following treatment with s50-TBG-RNAi-CK2. A1-C1, mice (5–8 per group) were enrolled when tumors were 3 to 4 mm diameter. s50-TBG-RNAi-CK2 nanocapsule treatment was administered by tail vein injection. The day of initial and repeated treatment (if given) is indicated by arrows on the x-axis. Tumor size is presented as mean ± S.D. Overall comparisons of tumor volumes at 35 days: SCC-15 p=0.003; UM-11b p=0.172; FaDu p<0.0001. A2-C2, survival was recorded during the more than six month study period. Overall log-rank test: SCC-15 p=0.008; UM-11b p=0.340; FaDu p<0.0001. *, RNAi-CK2 treatment groups that were significantly different from the vehicle, sense and sugar controls. ‡, s50-TBG-RNAi-CK2 treatment groups that were significantly different from the vehicle controls. A3–C3, confocal micrographs of Ago2 levels (red) in vehicle treated primary

xenograft tumors. Nuclei are counterstained with bisbenzamide (blue). Co-localized nuclear Ago2 and bisbenzamide stained nuclei display as pink in the merged images.

Table 1

Dose and survival response to s50 TBG-RNAi-CK2 in mice carrying various HNSCC tumors

SCC-15 (tongue carcinoma)[#]	**Dosage (mg/kg)**	**Dosing regimen**	**Number of Mice**	**6-month survival**	**Mice with tumor or metastasis signal**[a]
s50 TBG-RNAi-CK2	50 mg/kg	1×	8	6*	1
s50 TBG-RNAi-CK2	50 mg/kg	2× q 1 week	8	4	0
s50 TBG-Sense	50 mg/kg	1×	8	1	1
Vehicle		1×	8	1	1
UM-11b (laryngeal carcinoma)[§]					
s50 TBG-RNAi-CK2	50 mg/kg 25 mg/kg	1× ea q 48 hr	8	3	1
s50 TBG-RNAi-CK2	25 mg/kg	2× q 48 hr	8	6*	2
s50 TBG-Sense	25 mg/kg	2× q 48 hr	8	4	3
Vehicle		2× q 48 hr	8	6	6
FaDu (hypopharyngeal carcinoma)					
s50 TBG-RNAi-CK2	10 mg/kg	2× q 48 hr	8	3	1
s50 TBG-RNAi-CK2	0.01 mg/kg	2× q 48 hr	6	3*	1
s50 TBG-Sense	25 mg/kg	1×	8	0	No survivors
s50 TBG-Sugar	10 mg/kg	2× q 48 hr	5	0	No survivors
Vehicle		2× q 48 hr	8	0	No survivors

[a] Determined by luciferase imaging for all mice remaining in the survival study at 6 months as described previously[12].

* Comparison of lower to higher total s50-TBG-RNAi-CK2i dose, Log-Rank $p < 0.001$.

[#] Comparison of % surviving mice with tumor or metastases, Fisher's Exact $p = 0.118$.

[§] Comparison of % surviving mice with tumor or metastases, Fisher's Exact $p = 0.058$.